Quantum criticality and development of antiferromagnetic order in the quasikagome Kondo lattice CeRh$_{1-x}$Pd$_x$Sn

C. L. Yang,[1] S. Tsuda,[1] K. Umeo,[2] Y. Yamane,[1] T. Onimaru,[1] T. Takabatake,[1] N. Kikugawa,[3] T. Terashima,[3] and S. Uji[3]

[1]*Graduate School of Advanced Science of Matter, Hiroshima University, Higashi-Hiroshima, 739-8530, Japan*

[2]*Cryogenics and Instrumental Analysis Division, N-BARD, Hiroshima University, Higashi-Hiroshima 739-8526, Japan*

[3]*Research Center for Functional Materials, National Institute for Materials Science, Tsukuba, Ibaraki 305-0003, Japan*

CeRhSn with a quasikagome lattice of Ce atoms in the hexagonal c plane has been expected to be in close vicinity to a zero-field quantum criticality derived from magnetic frustration. We have studied how the ground state changes with substitution of Pd for Rh in CeRh$_{1-x}$Pd$_x$Sn ($x \leqslant 0.75$) by measuring the specific heat C, magnetic susceptibilities χ_{dc} and χ_{ac}, magnetization M, electrical resistivity ρ, and magnetoresistance. For $x = 0$, the field dependence of χ_{ac} at $T = 0.03$ K shows a peak at $B \parallel a = 3.5$ T, confirming the spin-flop crossover in the field applied along the hard axis. The temperature dependence of χ_{ac} shows a broad maximum at 0.1 K whereas C/T continues to increase down to 0.08 K. For $x \geqq 0.1$, $\rho(T)$ is dominated by incoherent Kondo scattering and both C/T and $\chi_{ac}(T)$ exhibit peaks, indicating the development of an antiferromagnetic order. The ordering temperature rises to 2.5 K as x is increased to 0.75. Our results indicate that the ground state in the quasikagome Kondo lattice CeRh$_{1-x}$Pd$_x$Sn leaves the quantum critical point at $x = 0$ with increasing x as a consequence of suppression of both the magnetic frustration and Kondo effect.

I. INTRODUCTION

In insulating systems with geometrically frustrated structures, a long-range magnetic order is suppressed by frustrated spin-spin interactions between the nearest and next nearest neighbors, leading to intriguing ground states, such as spin ices, spin glasses, and spin liquids [1,2]. In metallic 4f electron systems, on the other hand, the interaction between local moments is carried by conduction electrons, therefore the longer ranged interaction may make the magnetism partially suppressed by geometrical frustration [3,4]. The conventional quantum criticality in 4f electron systems at zero temperature can be reached by tuning the coupling between the 4f electron and conduction electrons governing the competition between the Kondo effect and Ruderman-Kittel-Kasuya-Yosida (RKKY) interaction, which is well known as the Doniach phase diagram [5]. The ordinary ways to tune the balance of the two interactions are through chemical composition, pressure, and magnetic field, leading from a magnetically ordered state to a paramagnetic one through a quantum critical point (QCP). Recently, an additional tuning parameter Q, which represents the quantum zero-point motion of spins induced by magnetic frustration, was introduced to describe the unconventional quantum criticality in the geometrical frustrated Kondo lattice [6–8]. Especially, a kagome Kondo lattice with antiferromagnetic (AFM) nearest-neighbor interaction due to the triangularlike geometry is expected to have unconventional QCPs and magnetic orders depending on the band filling fraction and the degree of Kondo coupling [9–11]. In this system, the competition occurs between a spin liquid state and a Kondo singlet state, which is caused by the interplay among the RKKY-interaction, Kondo effect, and magnetic frustration. Hence, a long-range AFM order can be induced by either destruction of symmetry of frustrated structure or breakdown of Kondo screening.

A well-studied heavy-fermion antiferromagnet with a quasikagome lattice is the Ising-like CePdAl with nearly trivalent Ce ions in the hexagonal ZrNiAl-type structure with no inversion symmetry [12]. Within a single quasikagome layer, only two thirds of Ce moments participate in the long-range AFM order at $T_N = 2.7$ K, while the others remain paramagnetic [13,14]. Application of magnetic field along the Ising c axis suppresses the AFM order and results in a sequence of phase transitions or crossovers that arise from the competition between Kondo screening and geometrical frustration [15–17]. Substitution of an isovalent element Ni for Pd in CePd$_{1-x}$Ni$_x$Al decreases the lattice parameter and thus enhances the Kondo effect [18–20]. Thereby, the AFM order is completely suppressed at $x = 0.144$. The ratio $|\theta_p|/T_N$, where θ_p is the paramagnetic Curie temperature in the magnetic susceptibility χ, increases with x as the Kondo effect surpasses the RKKY interaction. An opposite crossing of a QCP occurs in the isostructural alloy system CeRh$_{1-x}$Pd$_x$In, in which a valence-fluctuating state in CeRhIn changes to an AFM heavy fermion state with increasing x [21]. An AFM order appears only at a very high content $x = 0.8$ at $T_N = 0.65$ K, which rises to 1.7 K for $x = 1$. The crossing of a QCP is thought to be driven by the effect of the increase in the 4d-electron number. Thereby, the 4f level deepens from the Fermi level and thus weakens the hybridization between the Ce 4f state and Rh/Pd 4d states [21].

In the isostructural compound CeRhSn, layers composed of Ce and Rh1 atoms alternate along the c axis with layers composed of Rh2 and Sn atoms, as shown in the inset of Fig. 1 [22]. The Ce atom has nearest neighbors of four Rh2 atoms and second nearest neighbor of one Rh1 atom. This structural aspect suggested that the Ce 4f state is strongly hybridized with the 4d band derived mainly from the Rh2 atoms, leading to the valence-fluctuating state with a high Kondo temperature $T_K \sim 200$ K [23,24]. Below 7 K, the specific heat divided by temperature C/T turns up and is saturated to a large value of 200 mJ/K^2 mol at 0.5 K. However, non-Fermi liquid (NFL) behaviors were observed in $\chi(T)$ and the electrical resistivity $\rho(T)$ down to 0.5 K: $\chi(T)$ shows a power-law behavior, and $\rho(T)$ decreases with $T^n (n \leqslant 1.5)$. These NFL behaviors are
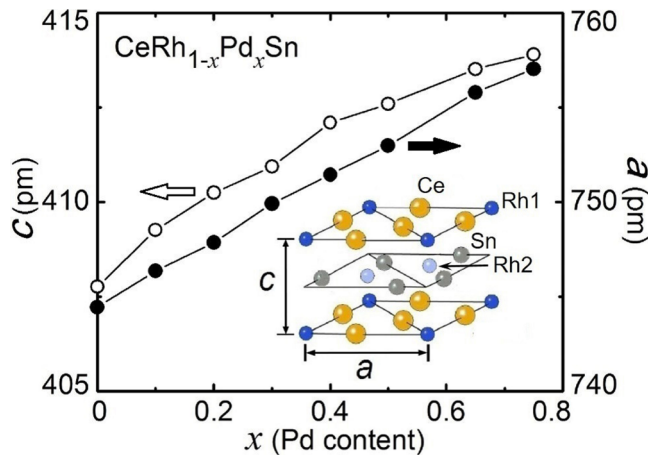
FIG. 1. Hexagonal lattice parameters a and c of $CeRh_{1-x}Pd_xSn$ as a function of x. The data except for $x = 0.1$ are derived from Ref. [28]. The inset shows the unit cell of CeRhSn.

thought to be a manifestation of the frustration of Ce moments, which hinders the long-range order [24]. In fact, no magnetic order down to 0.05 K was observed by muon spin relaxation (μSR) experiments [25]. Recently, measurements of C and uniaxial thermal expansion have been performed down to 0.06 K [26]. The anisotropic thermal expansion displaying the critical behavior only along the a axis is in support of the fact that the quantum criticality is driven by the geometrical frustration in the quasikagome lattice.

Motivated by the suggestion of zero-field QCP in CeRhSn, we have focused on the substituted system $CeRh_{1-x}Pd_xSn$ in which a magnetic order is expected to emerge at a smaller content of Pd than $x = 0.8$ in $CeRh_{1-x}Pd_xIn$ [21]. However, no magnetic order has been observed down to 2.5 K in the measurements of $\rho(T)$ and $\chi(T)$ for the alloys of $CeRh_{1-x}Pd_xSn$, which maintain the ZrNiAl-type structure up to $x = 0.8$ [27]. We expected that the destruction of the local symmetry of the frustrated structure by partial substitution should induce a magnetic order at low temperatures. Bearing this in mind, we have conducted magnetic, transport, and specific-heat measurements of the alloy system down to 0.03 K. A part of experimental results in Figs. 1, 4, and 5(a) has been reported in conference proceedings [28].

II. EXPERIMENTS

Polycrystalline samples with initial compositions of $CeRh_{1-x}Pd_xSn$ ($x = 0, 0.1, 0.2, 0.3, 0.4, 0.5, 0.7, 0.8$) were prepared by arc-melting appropriate amounts of constituent elements Ce (99.9%), Rh (99.9%), Pd (99.99%), and Sn (99.999%) under a purified argon atmosphere. In order to improve the homogeneity, the ingots were turned over and melted for several times and were subsequently annealed at 900°C for 6 days in evacuated quartz ampoules. Total weight loss after preparation was not more than 1%. The samples were characterized by metallographic examination, powder x-ray diffraction, and wavelength dispersive electron-probe micro-analysis (EPMA). The metallographic examination showed that the polycrystalline samples are composed of grains of approximately 500 μm in length preferentially oriented along

the c axis, which is perpendicular to the bottom surface of the ingot. The value of the Pd composition x determined by EPMA for polycrystalline samples of $CeRh_{1-x}Pd_xSn$ agrees with the nominal composition X in the range of $X \leqslant 0.5$. However, for $X > 0.5$, it was revealed that the quantity of impurity phase $Ce(Rh_{1-X}Pd_X)_2Sn_2$ increases to approximately 5%. This makes the Pd content x smaller than X, i.e., 0.65 and 0.75 for $X = 0.7$ and 0.8, respectively. Lattice parameters of the ZrNiAl-type structure were calculated by least-square re-finements of the XRD patterns. Single crystals $CeRh_{1-x}Pd_xSn$ ($x = 0$ and 0.1) were grown by the Czochralski method in an RF induction furnace with an argon gas atmosphere [24]. The compositions of both ends of the single crystals of 50 mm in length were examined by EPMA. No impurity phase nor deviation in the stoichiometry was detected within the 1% resolution.

For the measurements of $\rho(T), \chi_{ac}(T), \chi_{dc}(T), C(T)$, and magnetization $M(B)$, we used polycrystalline samples with long grains preferentially oriented along the c axis. Along this direction, the electric current and magnetic field were applied for $\rho(T)$ and $\chi_{ac}(T)$ measurements, respectively. Because the hexagonal compound CeRhSn exhibits uniaxial magnetic anisotropy, $\chi(B \parallel c) > \chi(B\perp c)$ [24], we measured $\chi_{dc}(T)$ for polycrystalline samples in two configurations with external fields parallel and perpendicular to the oriented direction. The averaged value, $\{\chi(B \parallel) + 2\chi(B\perp)\}/3$, was taken as χ_{dc} to minimize the effect of anisotropy. Single crystals with $x = 0$ and 0.1 were oriented along the a and c axes for the measurements of $\chi_{dc}(T)$ and $M(B)$, which were performed with a Quantum Design MPMS from 1.8 to 300 K and a homemade Faraday force magnetometer in a ^{3}He cryostat at temperatures down to 0.4 K. The temperature- and magnetic-field dependences of χ_{ac} were measured under $B_{ac} = 372\mu$T at the frequency of 67.2 Hz in an OXFORD ^{3}He$-^4$He dilution refrigerator at Tsukuba Magnet Laboratory, NIMS. The field dependences of $\rho(B)$ in both longitudinal and transverse configurations were measured by the ac method up to 17.5 T with the dilution refrigerator. The specific heat from 0.4 to 20 K was measured by the relaxation method in a Quantum Design PPMS while that from 0.08 to 0.7 K was measured using a laboratory-built system installed in an adiabatic demagnetization refrigerator, mF-ADR50.

III. RESULTS AND DISCUSSION

As x in $CeRh_{1-x}Pd_xSn$ increases from 0 to 0.75, the hexag-onal a parameter linearly increases, while the c parameter deviates from the Vegard's law, as shown in Fig. 1. The deviation is in agreement with the previous report [27] and hints a change in the $4f$ state from the valence-fluctuating state to the localized state with increasing x. The valence of Ce in CeRhSn was evaluated as 3.07 by the Ce$3d$ x-ray photoelectron spectroscopy (XPS) measurements [29]. The possible change in the valence is 0.07 in $CeRh_{1-x}Pd_xSn$ as the valence becomes trivalent for $x = 0.75$, as will be described below in terms of the results of $\chi(T)$ and $M(B)$. The localized magnetic moments in the trivalent state may stabilize a magnetic order at low temperatures. The expansion along the c axis elongates the distance between the Ce and Rh2 atoms out of the basal plane, which may decrease the
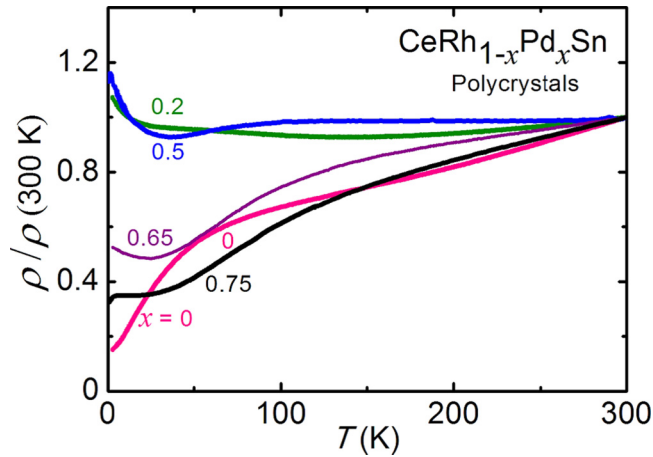
FIG. 2. Temperature dependence of electrical resistivity normalized to the value at 300 K for polycrystalline samples of $CeRh_{1-x}Pd_xSn$.

FIG. 3. Temperature dependence of the inverse of the averaged magnetic susceptibility of $CeRh_{1-x}Pd_xSn$ (see text). Solid lines are the fits with the modified Curie-Weiss form $\chi - \chi_0 = C/(T - \theta_p)$ to the data at temperatures above 100 K.

overlap of wave functions between the $4f$ electron and the $4d$ electron. In addition, local extension near the substituted Pd atom may break the symmetry of the quasikagome lattice of Ce atoms.

Figure 2 shows the electrical resistivity normalized to the value at 300 K, $\rho(T)/\rho(300\,\mathrm{K})$, for polycrystalline samples of $CeRh_{1-x}Pd_xSn$ ($x = 0, 0.2, 0.5, 0.65, 0.75$). The electrical current I was applied along the bar-shaped samples composed of grains preferentially oriented along the c axis. The values of $\rho(300\,\mathrm{K})$ are in the range between 80 and 140 $\mu\Omega$ cm. For $x = 0$, $\rho(T)$ displays a broad shoulder around 50 K followed by a decrease, in which the behavior resembles that of the single crystal for $I \parallel c$ shown in Fig. 9. For $x = 0.2$ and 0.5, a flat behavior is followed by an upturn at $T < 20$ K, which is likely attributed to incoherent Kondo scattering due to the disorder in the Kondo lattice. With further increasing x to 0.65, a metallic behavior is recovered. For $x = 0.75$, the decrease in $\rho(T)$ at $T < 5$ K hints a sort of magnetic order at lower temperatures.

The dramatic change in the $4f$ state with Pd substitution is expected to manifest itself in the temperature dependent $\chi(T)$. As described above, $\chi(T)$ is the average $\{\chi(B \parallel) + 2\chi(B\perp)\}/3$, where $\chi(B \parallel)$ and $\chi(B\perp)$ were measured, respectively, in external fields of 1 T applied parallel and perpendicular to the sample preferentially oriented along the c axis. The inverse of $\chi - \chi_0$ vs T is plotted in Fig. 3, where the solid lines for $T > 100$ K are the fits to the data with the modified Curie-Weiss form $(\chi - \chi_0)^{-1} = (T - \theta_p)/C$, where θ_p is the paramagnetic Curie temperature and χ_0 represents the temperature independent contribution. The parameters of fitting are listed in Table I. For $x = 0$, the large and negative value of $\theta_p = -155$ K and the small effective magnetic moment $\mu_{\mathrm{eff}} = 1.42\mu_B$ are characteristics of a valence-fluctuating Ce compound. With the increase in x to 0.5, $|\theta_p|$ gradually decreases to 23 K. This decreasing trend in $|\theta_p|$ is understood as the decreasing of T_K because $|\theta_p|/2$ is a measure of T_K in the absence of frustration effects [30]. For $x \geqslant 0.65$, μ_{eff} increases nearly to $2.54\mu_B$, which is the expected value for a free Ce^{+3} ion. As shown in the inset of Fig. 4, $\chi(B \parallel)$
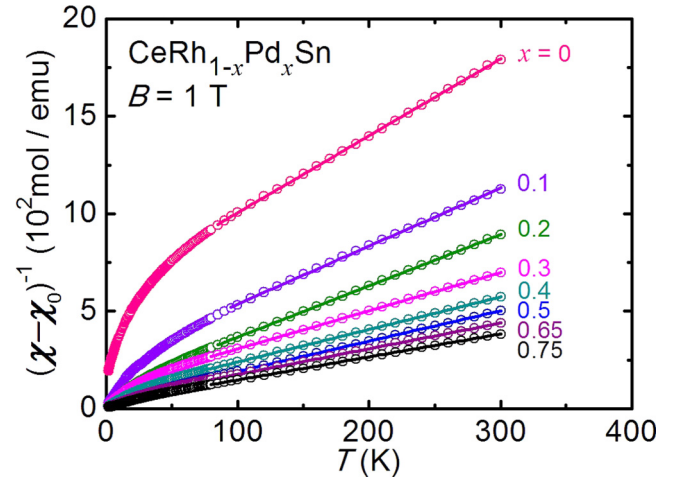
for $x = 0.75$ exhibits a maximum at around 3 K, suggesting an AFM order. We note that the magnetic order at round 3 K is not due to the impurity phase of $Ce(Rh_{1-x}Pd_x)_2Sn_2$ because both end compounds $CeRh_2Sn_2$ and $CePd_2Sn_2$ order antiferromagnetically only below 0.5 K [31].

The isothermal magnetization curves $M(B \parallel)$ of polycrystals measured in fields up to 5 T at $T = 1.8$ K are shown in Fig. 4. For $x = 0$, $M(B \parallel)$ increases almost linearly, reaching a value of $0.05\mu_B$/Ce at 5 T. This value is 67% of the reported value for the single crystal for $B \parallel c$ [24], confirming the preferred orientation of grains along the c axis in the polycrystal. For $x \geqslant 0.1$, $M(B)$ gradually increases and shows a tendency towards saturation. It is noteworthy that $M(B \parallel)$ for $x = 0.75$ shows a spin-flop-like behaviour at $B = 2$T and reaches a saturated value of $1.4\mu_B$/Ce at 5 T. This magnitude is close to the saturation moment along the easy c axis in CePdAl with nearly trivalent Ce ions [15].

TABLE I. Parameters obtained by the fits with the modified Curie-Weiss form $\chi = C/(T - \theta_p) + \chi_0$ to the averaged magnetic susceptibility data $\{\chi(B \parallel) + 2\chi(B\perp)\}/3$ at $T > 100$ K, where $\chi(B \parallel)$ and $\chi(B\perp)$ were measured, respectively, in external fields of 1 T applied parallel and perpendicular to the samples of $CeRh_{1-x}Pd_xSn$ preferentially oriented along the c axis. μ_{eff}, θ_p, and χ_0 are the effective magnetic moment, paramagnetic Curie temperature, and temperature independent term, respectively.

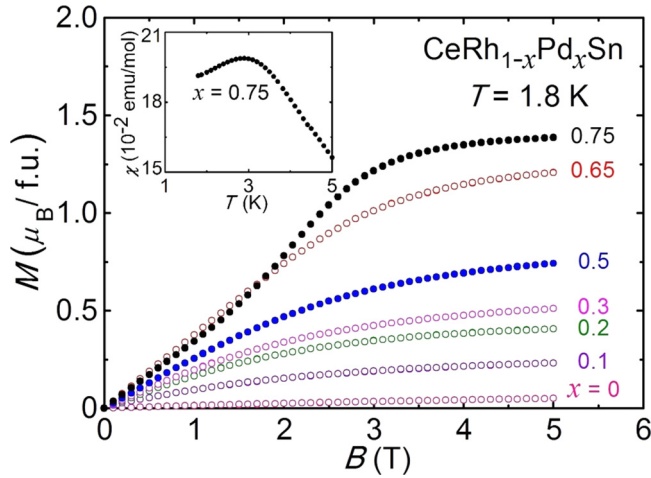| Pd content x	Effective moment $\mu_{\mathrm{eff}}(\mu_B/\mathrm{Ce})$	Paramag. Curie temp. θ_p (K)	$\chi_0(10^{-4}\mathrm{mol/emu})$
0	1.42	−155	7.37
0.1	1.64	−80	7.20
0.2	1.74	−40	6.29
0.3	2.02	−57	5.20
0.4	2.19	−43	3.51
0.5	2.27	−23	2.80
0.65	2.47	−34	1.18
0.75	2.60	−25	0

FIG. 4. Isothermal magnetization curves $M(B \parallel)$ of polycrystalline samples of $CeRh_{1-x}Pd_xSn$ as a function of the magnetic field at 1.8 K. The data except for $x = 0.1$ are derived from Ref. [28]. The inset shows the temperature dependence of the magnetic susceptibility for $x = 0.75$ below 5 K.

Emergence of magnetic order in $CeRh_{1-x}Pd_xSn$ has been revealed by the measurements of specific heat $C(T)$ and $\chi_{ac}(T)$ down to 0.08 K and 0.03 K, respectively. The data of C/T are plotted vs $\log T$ in Fig. 5(a), where C/T for $x = 0$ weakly increases on cooling, as was reported [26]. On the contrary, C/T for $x = 0.1$ exhibits $-\log T$ dependence, which is followed by a maximum at $T_M = 0.1$ K, suggesting the onset of a magnetic order. The peak temperature T_M increases to 1.0 K with the increase in x to 0.5, where the peak of C/T becomes highest. For $x = 0.75$, two humps are found at 1.2 K and 2.5 K, the latter of which is adopted as T_M because it agrees with the maximum temperature of $\chi_{dc}(B \parallel)$, as seen in the inset of Fig. 4. Similarly, $\chi_{ac}(T)$ plotted in Fig. 5(b) shows a maximum at T_χ, whose temperature shifts from 0.1 to 0.7 K as x is increased from 0 to 0.4. It is noteworthy that χ_{ac} for $x = 0$ shows a maximum at 0.1 K, whereas C/T does not exhibit a peak down to 0.07 K. The different behaviors might be interpreted as the manifestation of a spin glass state. It is, however, at variance with the absence of any kind of magnetic order down to 0.05 K, as proved by μSR measurements [25]. The nature of the ground state in $CeRh_{1-x}Pd_xSn$ has to be further clarified by microscopic methods with respect to exotic magnetic orderings proposed for kagome Kondo lattice as functions of electron density and Kondo coupling [9–11].

Here, we recall that the field dependence of C/T measured at 0.07 K for the single crystal with $x = 0$ showed a peak at 3.6 T only when the external field was applied along the a axis [26]. It was inferred as the evidence for the spin-flop crossover in the frustrated state. In order to examine this proposition, we have measured field dependence of χ_{ac} in $B \parallel a$ and $B \parallel c$ at various constant temperatures. As shown in Fig. 6, $\chi_{ac}(Bc)$ at 0.05 K has no anomaly, whereas $\chi_{ac}(B \parallel a)$ at 0.03 K exhibits a peak at 3.5 T, in agreement with the field dependence of C/T. With increasing temperature to 0.62 K, the peak broadens and seems to separate into two maxima, as observed in C/T. Our observations support the proposition of spin-flop crossover of frustrated Ce moments in the ground state [26].
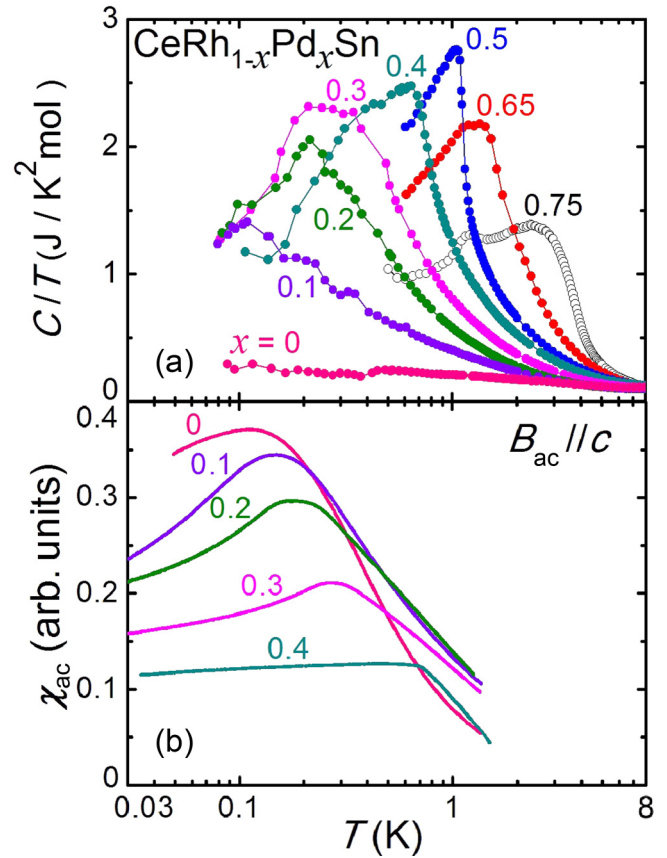

FIG. 5. (a) Specific heat of polycrystalline samples of $CeRh_{1-x}Pd_xSn$ ($0 \leqslant x \leqslant 0.75$) plotted as C/T vs $\log T$. (b) The ac magnetic susceptibility vs $\log T$ for single crystals with $x = 0$ and 0.1 and polycrystals with 0.2, 0.3, and 0.4.
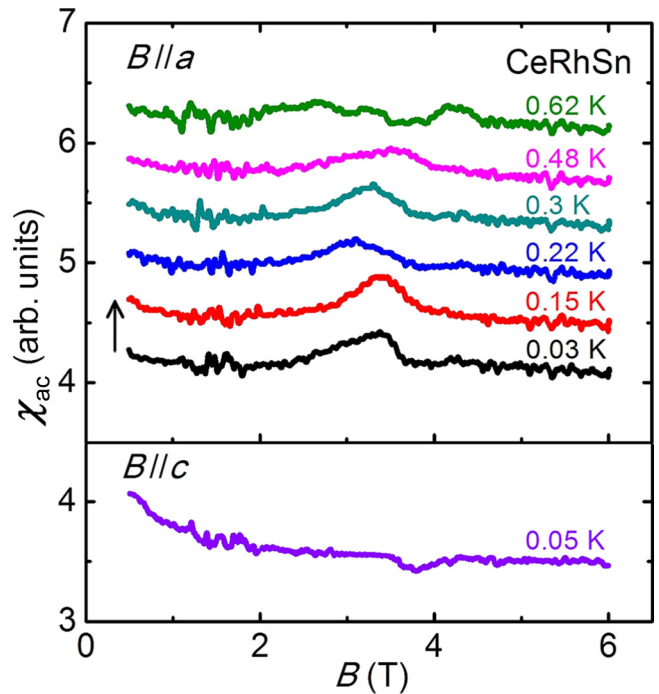

FIG. 6. Isothermal ac susceptibility of the CeRhSn single crystal as a function of magnetic field B applied parallel to the a and c axes, respectively. The data are vertically shifted for clarity.
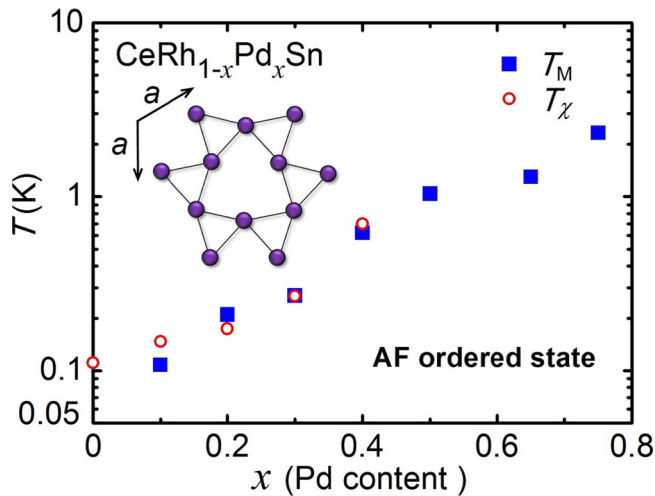
FIG. 7. Temperatures at the maximum in C/T (■) and $\chi_{ac}(T)$ (○) for $CeRh_{1-x}Pd_xSn$ vs x.

FIG. 8. Magnetic entropy of $CeRh_{1-x}Pd_xSn$ as a function of temperature. The dashed line represents the value of $0.65R\ln2$.

The temperatures of T_M and T_χ are plotted in Fig. 7, constructing a phase diagram of $CeRh_{1-x}Pd_xSn$. For $x = 0.1$, T_χ is higher than T_M but T_χ agrees with T_M in the range $0.2 \leqslant x \leqslant 0.4$. The increasing trend of T_M and T_χ suggests that the Pd substitution for Rh suppresses both frustration and Kondo effect, leading to the development of an AFM order. From the bulk measurements presented here, however, it is difficult to separate the two contributions from frustration and Kondo effect. The effect of frustration on the magnetic structure in this system could be elucidated by neutron scattering experiments, as was successfully done for CePdAl [13,19].

In order to estimate the magnetic entropy $S(T)$, the data of C/T of $CeRh_{1-x}Pd_xSn$ for $x = 0$ and $0.1 \leqslant x \leqslant 0.75$ were tentatively extrapolated to $T = 0$ by using the equations $C/T = \gamma + \beta T^2 + CT^2\ln T$ and $C/T = \gamma + \beta T^2 + \delta T^2 e^{-\Delta/k_B T}$, respectively, which are relevant for a spin-fluctuating system and an antiferromagnet with spin wave excitations with an anisotropic gap [32,33]. The data of isostructural LaRhSn were used as the phonon contribution to be subtracted from the measured data. We calculated $S(T)$ by integrating the magnetic contribution to C/T and plotted the results in Fig. 8. The $S(T)$ curves for $x = 0.65$ and 0.75 are saturated to $R\ln2$ at around 10 K, confirming the doublet ground state of the Ce ion at the $3f$ site with the local $m2m$ symmetry under the crystal field. If we neglect the effect of frustration, then T_K can be estimated by using a relation for a Kondo impurity, $S(T_K) = 0.45 = 0.65\ln2$ [34]. The estimated T_K decreases from 80 K for $x = 0$ to 3 K for $x = 0.5$.

The ground state properties for $x = 0$ and $x = 0.1$ have been further studied by the measurements of $\rho(T), \chi(T)$, and magnetoresistance (MR) on single crystals. Figure 9 shows $\rho(T)$ for the current directions $I//a$ and $I//c$. The data for $x = 0$, which are derived from Ref. [24], exhibit large anisotropy $\rho_a(T) > \rho_c(T)$ and a maximum in $\rho_a(T)$ at around 70 K. The successive decrease in $\rho_a(T)$ on cooling is a characteristic of a Ce-based Kondo compound in the coherent scattering regime. For $x = 0.1$, the large anisotropy is maintained, but the maximum in $\rho_a(T)$ is absent, as seen in the inset where the magnetic part is replotted vs $\ln T$. The continuous increase in
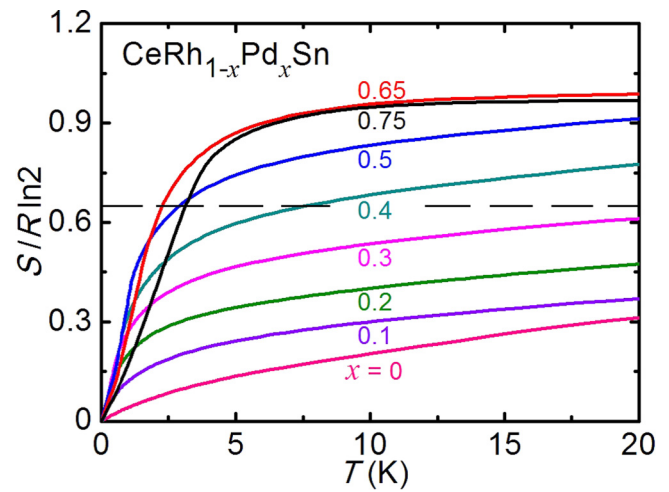
$\rho_a(T)$ down to 1.5 K is attributed to the loss of coherence in the quasikagome Kondo lattice by atomic disorder. The weak upturn in both $\rho_a(T)$ and $\rho_c(T)$ at temperatures below 20 K is similar to that observed in the polycrystalline sample with $x = 0.2$ in Fig. 2.

Figure 10 represents a double logarithmic plot of dc susceptibility $\chi(T)$ for single crystals with $x = 0$ and 0.1 in a field of 0.1 T applied $//a$ and $//c$. The large anisotropy $\chi_c(T) \gg \chi_a(T)$ is maintained for $x = 0.1$, which is similar for $x = 0$ [24]. In the temperature range 0.8–5 K, $\chi_c(T)$ and $\chi_a(T)$ for $x = 0$ follow the power law $\chi(T) \propto T^{-n}$ with $n = 1.1$ and 0.35, respectively [24]. The values of n for $x = 0.1$ converge to 0.6 for both $\chi_c(T)$ and $\chi_a(T)$. As shown in the inset, $M(B \parallel c)$ at 0.3 K reaches a value of $0.32 \mu_B$/f.u., being four times larger than that of $M(B \parallel a)$. The magnitude of $M(B \parallel a)$ for $x = 0.1$ is comparable with that of $M(B \parallel c)$ for $x = 0$.
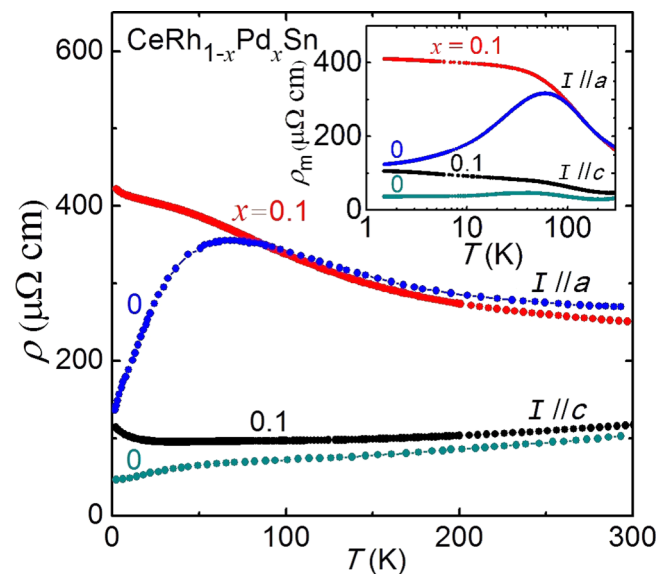

FIG. 9. Electrical resistivity of single crystals $CeRh_{1-x}Pd_xSn$ with $x = 0$ and 0.1 for the current I parallel to the a and c axes, respectively. The data for $x = 0$ are derived from Ref. [24]. The inset shows the magnetic contribution to the resistivity vs $\log T$.
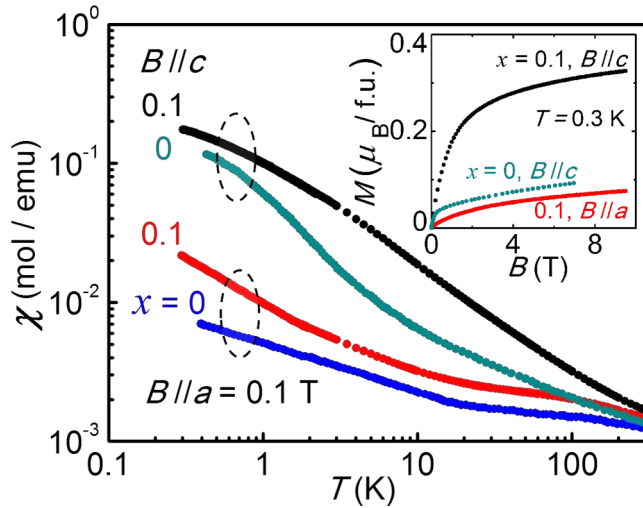
FIG. 10. The dc magnetic susceptibility of single crystals of CeRh$_{1-x}$Pd$_x$Sn with $x = 0$ and 0.1 for $B \parallel a$ and $B \parallel c$, respectively. The inset shows the isothermal magnetization for $B \parallel a$ and $B \parallel c$ at 0.3 K. The data for $x = 0$ are derived from Ref. [24].

The MR was measured at various constant temperatures. Figure 11 represents the relative MR, $\{\rho(B) - \rho(B = 0)\}/\rho(B = 0)$, measured at the lowest temperature 0.08 K for the configurations $B \parallel I$ and $B \perp I$. For $x = 0$, MRs in the
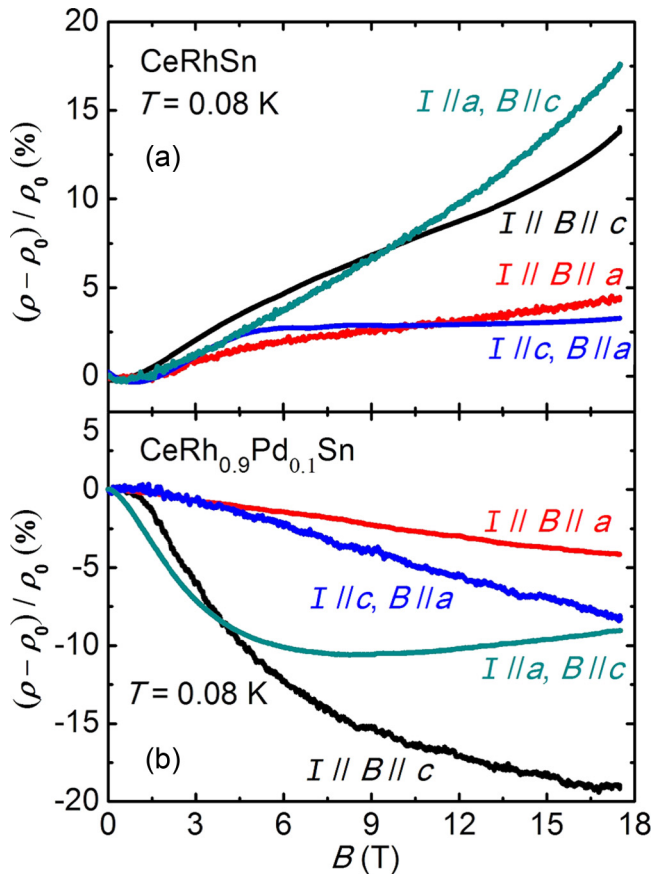

FIG. 11. Normalized magnetoresistance for single crystals CeRh$_{1-x}$Pd$_x$Sn with $x = 0$ (a) and $x = 0.1$ (b) at 0.08 K in applied fields $B \parallel a$ and $B \parallel c$ for the longitudinal and transverse configurations.

four configurations are all positive. The fact that the values of MR($I \parallel a, B \parallel c$) and MR($I \parallel c, B \parallel c$) are comparable is an indication for the positive MRs not being originated from cyclotron motions of conduction electrons because cyclotron motions occur only under $B \perp I$. A positive MR for $B \parallel I$ is expected to appear for a Ce-based heavy fermion system with a gaplike structure above the Fermi level [35]. It is actually observed for a valence-fluctuating compound CePd$_3$ [36] and a heavy fermion compound CeRu$_2$Si$_2$ [37]. Therefore, the observed positive MR for $x = 0$ is likely to be the characteristic of the gaplike structure in coherent Kondo lattice compounds. The change in the slope of MR at around $B \parallel a = 4$ T may be originated from the spin-flop crossover that appeared in the field dependence of C/T and χ_{ac}. On the contrary, MRs for $x = 0.1$ are all negative, as shown in Fig. 11(b). The absolute value of MR for $I \parallel B \parallel c$ at 8 T is approximately five times larger than that for $I \parallel B \parallel a$, in which the relation is similar with that of $M(B \parallel c) \cong 5M(B \parallel a)$, as shown in the inset of Fig. 10. This correlation between the MR and magnetization indicates that the negative MR is caused by the field-induced suppression of impurity Kondo scattering [38]. We also measured $\rho(T)$ under various constant magnetic fields and found that the negative MR for $B \parallel c$ becomes significant at $T < 10$ K. In this temperature range, $\rho(T)$ for both $I \parallel a$ and $I \parallel c$ turns up on cooling as shown in Fig. 9.

IV. CONCLUSION

Magnetic frustration in the quasikagome lattice of Ce atoms in the c plane of CeRhSn has been expected to place this compound near the QCP. In order to confirm this expectation and to study how the ground state changes in CeRh$_{1-x}$Pd$_x$Sn, we have measured the magnetic, transport, and thermal properties at temperatures down to 0.03 K. It is found that χ_{ac} for $x = 0$ shows a broad maximum at 0.1 K, whereas C/T keeps increasing down to 0.07 K. Upon applying magnetic fields along the a axis, $\chi_{ac}(B)$ at 0.03 K exhibits a peak at 3.5 T, which is consistent with the peak observed in C/T at 3.6 T. The metamagnetic behavior in the field applied along the hard axis is attributed to destruction of magnetic frustration among Ce moments in the c plane. This confirms that the frustration hinders the long-range magnetic order in CeRhSn. The maximum in $\rho(T)$ due to coherent scattering disappears for $x \geqslant 0.1$ and both C/T and $\chi_{ac}(T)$ exhibit a maximum, whose temperature increases from 0.1 K for $x = 0.1$ to 2.5 K for $x = 0.75$. Thereby, the magnetic entropy at 20 K increases from $0.36R\ln2$ to $0.96R\ln2$, indicating the full recovery of the magnetic freedom of the doublet ground state. It is naively conjectured that the quantum effect on the frustration is weakened in a fully localized moment state of $J = 5/2$ than in a reduced moment state for $x < 0.1$. We infer that the appearance of magnetic order in CeRh$_{1-x}$Pd$_x$Sn for $x \geqslant 0.1$ is the consequence of suppressions of the Kondo effect and magnetic frustration. The role of frustration in the phase diagram needs to be further studied by microscopic experiments such as neutron scattering and NMR. All our observations corroborate that the ground state of the quasikagome Kondo lattice CeRhSn is very close to the QCP resulting from the interplay among Kondo effect, RKKY interaction, and geometrical frustration.

ACKNOWLEDGMENTS

[1] L. Balents, Nature (London) **464**, 199 (2010).

[2] *Introduction to Frustrated Magnetism: Materials, Experiments, Theory*, edited by C. Lacroix, P. Mendels, and F. Mila (Springer, Heidelberg, 2011).

[3] C. Lacroix, J. Phys. Soc. Jpn. **79**, 011008 (2010).

[4] B. H. Bernhard, B. Coqblin, and C. Lacroix, Phys. Rev. B **83**, 214427 (2011).

[5] S. Doniach, Physica B **91**, 231 (1977).

[6] M. Vojta, Phys. Rev. B **78**, 125109 (2008).

[7] P. Coleman and A. H. Nevidomskyy, J. Low Temp. Phys. **161**, 182 (2010).

[8] Q. Si, J. H. Pixley, E. Nica, S. J. Yamamoto, P. Goswami, R. Yu, and S. Kirchner, J. Phys. Soc. Jpn. **83**, 061005 (2014).

[9] K. Barros, J. W. F. Venderbos, G.-W. Chern, and C. D. Batista, Phys. Rev. B **90**, 245119 (2014).

[10] H. Ishizuka and Y. Motome, Phys. Rev. B **91**, 085110 (2015).

[11] S. Ghosh, P. O'Brien, C. L. Henley, and M. J. Lawler, Phys. Rev. B **93**, 024401 (2016).

[12] H. Kitazawa, A. Matsushita, T. Matsumoto, and T. Suzuki, Physica B **199–200**, 28 (1994).

[13] A. Dönni, G. Ehlers, H. Maletta, P. Fischer, H. Kitazawa, and M. Zolliker, J. Phys.: Condens. Matter **8**, 11213 (1996).

[14] A. Oyamada, S. Maegawa, M. Nishiyama, H. Kitazawa, and Y. Isikawa, Phys. Rev. B **77**, 064432 (2008).

[15] T. Goto, S. Hane, K. Umeo, T. Takabatake, and Y. Isikawa, J. Phys. Chem. Solids **63**, 1159 (2002).

[16] H. C. Zhao, J. H. Zhang, S. L. Hu, Y. Isikawa, J. L. Luo, F. Steglich, and P. J. Sun, Phys. Rev. B **94**, 235131 (2016).

[17] S. Lucas, K. Grube, C.-L. Huang, A. Sakai, W. Wunderlich, E. L. Green, J. Wosnitza, V. Fritsche, P. Gegenwart, O Stokert, and H. v. Löhneysen, Phys. Rev. Lett. **118**, 107204 (2017).

[18] V. Fritsch, N. Bagrets, G. Goll, W. Kittler, M. J. Wolf, K. Grube, C. L. Huang, and H. v. Löhneysen, Phys. Rev. B **89**, 054416 (2014).

[19] V. Fritsch, O. Stockert, C.-L. Huang, N. Bagrets, W. Kittler, C. Taubenheim, B. Pilawa, S. Woitschach, Z. Huesges, S. Lucas, A. Schneidewind, K. Grube, and H. v. Löhneysen, Eur. Phys. J. Spec. Top. **224**, 997 (2015).

[20] A. Sakai, S. Luchas, P. Gegenwart, O. Stockert, H. v. Löhneysen, and V. Fritsch, Phys. Rev. B **94**, 220405(R) (2016).

[21] E. Brück, H. Nakotte, K. Bakker, F. R. de Boer, P. F. de Châtel, J.-Y. Li, J. P. Kuang, and F.-M. Yang, J. Alloys Comp. **200**, 79 (1993).

[22] R. Mishra, R. Pöttgen, R.-D. Hoffman, H. Trill, B. D. Mosel, H. Piotrowski, and M. F. Zumdick, Z. Naturforsch. **56b**, 589 (2001).

[23] A. Ślebarski, M. B. Maple, E. J. Freeman, C. Sirvent, M. Radłowska, A. Jezuerski, E. Granado, Q. Huang, and J. W. Lynn, Phil. Mag. B **82**, 943 (2002).

[24] M. S. Kim, Y. Echizen, K. Umeo, S. Kobayashi, M. Sera, P. S. Salamakha, O. L. Sologub, and T. Takabatake, Phys. Rev. B **68**, 054416 (2003).

[25] A. Schenck, F. N. Gygax, M. S. Kim, and T. Takabatake, J. Phys. Soc. Jpn. **73**, 3099 (2004).

[26] Y. Tokiwa, C. Stingl, M. S. Kim, T. Takabatake, and P. Gegenwart, Sci. Adv. **1**, e1500001 (2015).

[27] O. Niehaus, P. M. Abdala, and R. Pöttgen, Z. Naturforsch. **70**, 253 (2015).

[28] C. L. Yang, K. Umeo, and T. Takabatake, J. Phys.: Conf. Ser. **807**, 042001 (2017).

[29] M Gamza, A. Slebarski, and H. Resner, Eur. Phys. J. B **67**, 483 (2009).

[30] D. Gignoux and J. C. Gomez-Sal, Phys. Rev. B **30**, 3967 (1984).

[31] W. P. Beyermann, M. F. Hundley, P. C. Canfield, J. D. Thompson, M. Latroche, C. Godart, M. Selsane, Z. Fisk, and J. L. Smith, Phys. Rev. B **43**, 13130 (1991).

[32] M. B. Brodsky, Rep. Prog. Phys. **41**, 1547 (1978).

[33] B. R. Cooper, Proc. Phys. Soc. **80**, 1225 (1962).

[34] H.-U Desgranges and K. D. Schotte, Phys. Lett. A **91**, 240 (1982).

[35] N. Kawakami and A. Okiji, J. Phys. Soc. Jpn. **55**, 2114 (1986).

[36] M. Houshiar, D. T. Adroja, and B. D. Rainford, Physica B **223–224**, 268 (1996).

[37] S. Kambe, H. Suderow, J. Flouquet, P. Haen, and P. Lejay, Solid State Commun. **95**, 449 (1995).

[38] P. Schlottman, Z. Phys. B **51**, 223 (1983).